In vivo assessment of optimal *b*-value range for perfusion-insensitive apparent diffusion coefficient imaging

Moti Freiman,[a] Stephan D. Voss, Robert V. Mulkern, Jeannette M. Perez-Rossello, Michael J. Callahan, and Simon K. Warfield
Moti Freiman, Computational Radiology Laboratory, Department of Radiology, Boston Children's Hospital, Harvard Medical School, 300 Longwood Avenue, Boston Massachusetts 02115

(Received 8 December 2011; revised 8 June 2012; accepted for publication 12 June 2012; published 20 July 2012)

Purpose: To assess the optimal *b*-values range for perfusion-insensitive apparent diffusion coefficient (ADC) imaging of abdominal organs using short-duration DW-MRI acquisitions with currently available ADC estimation methods.
Methods: DW-MRI data of 15 subjects were acquired with eight *b*-values in the range of 5–800 s/mm^2. The reference-standard, a perfusion insensitive, ADC value (ADC_{IVIM}), was computed using an intravoxel incoherent motion (IVIM) model with all acquired diffusion-weighted images. Simulated DW-MRI data was generated using an IVIM model with *b*-values in the range of 0–1200 s/mm^2. Monoexponential ADC estimates were calculated using: (1) Two-point estimator (ADC_2); (2) least squares three-point (ADC_3) estimator and; (3) Rician noise model estimator (ADC_R). The authors found the optimal *b*-values for perfusion-insensitive ADC calculations by minimizing the relative root mean square error (RRMS) between the ADC_{IVIM} and the monoexponential ADC values for each estimation method and organ.
Results: Low *b*-value = 300 s/mm^2 and high *b*-value = 1200 s/mm^2 minimized the RRMS between the estimated ADC and the reference-standard ADC_{IVIM} to less than 5% using the ADC_3 estimator. By considering only the *in vivo* DW-MRI data, the combination of low *b*-value = 270 s/mm^2 and high *b*-value of 800 s/mm^2 minimized the RRMS between the estimated ADC and the reference-standard ADC_{IVIM} to <7% using the ADC_3 estimator. For all estimators, the RRMS between the estimated ADC and the reference standard ADC correlated strongly with the perfusion-fraction parameter of the IVIM model ($r = [0.78–0.83]$, $p \leq 0.003$).
Conclusions: The perfusion compartment in DW-MRI signal decay correlates strongly with the RRMS in ADC estimates from short-duration DW-MRI. The impact of the perfusion compartment on ADC estimations depends, however, on the choice of *b*-values and estimation method utilized. Likewise, perfusion-related errors can be reduced to <7% by carefully selecting the *b*-values used for ADC calculations and method of estimation. © *2012 American Association of Physicists in Medicine*. [http://dx.doi.org/10.1118/1.4736516]

Key words: diffusion-weighted imaging, *b*-value optimization, apparent diffusion coefficient, intravoxel incoherent motion

I. INTRODUCTION

Diffusion-weighted MRI (DW-MRI) is a noninvasive imaging technique sensitive to thermally driven motion of water molecules inside the body. This motion is usually represented with a monoexponential model with the apparent diffusion coefficient (ADC) as its parameter.[1] The ADC plays an increasingly important role as a quantitative biomarker for many clinical applications including its ability to differentiate between benign and malignant lesions;[2] evaluate tumor aggressiveness;[3] perform early assessment of tumor response-to-therapy;[4–6] evaluate the extent of liver fibrosis;[7–9] and assess the extent of Crohn's disease[10,11] as well as other diseases that are best evaluated with DW-MRI. Moreover, accurate estimates of ADC have been demonstrated as critical to diagnosing, evaluating, and monitoring these pathologies with precision.[12–14]

Depending on the acquisition parameters, *in vivo* measurements of the DW-MRI signal decay and its associated ADC can reflect a slow diffusion component associated with the Brownian motion of water molecules combined with a fast diffusion component associated with the bulk motion of intravascular molecules in the tissue micro capillaries.[15,16] When using the monoexponential model, however, this combination may produce an overestimate of the ADC values.

While the more complex intravoxel incoherent motion (IVIM) model[17] is able to separate the diffusion compartment from the micro capillaries' blood flow; this technique requires long-duration acquisitions with multiple *b*-value DW-MRI to encompass the wide range of fast diffusion decay due to perfusion, and similarly, slow diffusion decay due to pure diffusion.[18]

Such extended imaging, however, is not always desirable or feasible in routine clinical imaging, as increased scan times needed to acquire multiple *b*-values may likewise prolong sedation or anesthesia, and may result in poor image quality due to motion artifact.[16] Short-duration DW-MRI acquisitions

capable of providing accurate, perfusion-insensitive, ADC estimates are therefore of broad clinical interest.

Yamada *et al.*,[19] for example, suggest using intermediate and high *b*-values (e.g., 300 and 1100 s/mm^2, respectively) to approximate true diffusion using the monoexponential model while Padhani *et al.*[20] suggest using a lower *b*-value $\geq$ 100 s/mm^2 to obtain perfusion-insensitive ADC measurements. However, these studies are limited by the fact that neither performed a detailed quantitative analysis to identify optimal *b*-values. Although several papers have examined the choice of *b*-values for ADC calculations by evaluating the performance of the estimated ADC as a quantitative biomarker for various applications (usually for a specific pathology);[12–14] these analyses may represent overfitting of the *b*-values to the clinical diagnostic question rather than to the pure diffusion measurements which are of interest. Moreover, the above-mentioned studies were limited to a specific ADC estimation method—most often the two-point estimator for two *b*-value images[12,21] or the least-squares estimator for more than two *b*-value images.[12–14] Recently, several groups have shown that the accuracy of parameter estimates may be improved by using a Rician noise model to approximate the actual noise in diffusion-weighted MRI, though this approach may, at the same time, increase the variance of the estimates.[22–24] Specifically, Walker-Samuel *et al.* have demonstrated that by maximizing a Rician likelihood function, body DW-MRI can produce ADC estimates that are more accurate (but with higher variance) than the least squares estimator, which implicitly assumes a Gaussian noise model.[25]

In our experiment, we set out to quantitatively identify the range of *b*-values that provide ADC estimates of abdominal organs, less contamination from perfusion phenomena. We then compared our results to diffusion measurements from the IVIM model, specifically against the various ADC estimation methods in current clinical use.

II. MATERIALS AND METHODS

We carried out the study according to a protocol approved by our Institutional Review Board. MRI was retrospectively collected from 15 subjects [Nine males and six females with a mean age of 14.13 (range 7–24, std 4.09)] that underwent an abdominal MRI study between September 2010 and March 2011 due to suspected Crohn's disease. Abdominal organ findings in these subjects were normal.

II.A. MR imaging acquisition

The MRI imaging data of the abdomen was acquired using a 1.5 T unit (Magnetom Avanto, Siemens Medical Solutions, Erlangen, Germany) and a body-matrix coil and spine array coil for signal reception. The data were acquired with a free-breathing single-shot echo-planar imaging sequence using the following parameters: repetition time/echo time (TR/TE) = 6800/59 ms; SPAIR fat suppression; matrix size = 192 $\times$ 156; field of view = 300 $\times$ 260 mm; slice thickness/gap = 5 mm/0.5 mm; nominal diffusion time (Δ) = 25 ms; maximum gradient amplitude (G_{max}) = 2 G/cm; 40 axial slices; 8 *b*-values = 5,50,100,200,270,400,600,800 s/mm^2 with 1 average. To acquire four images at each *b*-value with an overall scan acquisition time of 4 min, a tetrahedral gradient scheme first proposed by Conturo *et al.*[26] was used. Next, trace-weighted diffusion images at each *b*-value were generated using geometric averages of the images acquired in each diffusion sensitization direction.[27]

II.B. Quantitative MR image analysis

II.B.1. Reference-standard diffusion measurements

The IVIM model, first introduced by Le Bihan,[17] accounts for both diffusion and perfusion effects on the signal decay

$$s_i = s_0(f\exp(-b_i(D^* + D)) + (1 - f)(\exp(-b_i D))) \quad (1)$$

where s_i is the observed signal with *b*-value:b_i; s_0 is the baseline signal (without any diffusion attenuation); f is the perfusion fraction; D^* is the perfusion compartment; and D is the diffusion coefficient. We estimated the model parameters for each voxel, using eight *b*-value images that were acquired with the estimation method proposed by Freiman *et al.*[28] Finally, we defined the IVIM model D parameter, which represents the perfusion-insensitive diffusion compartment, as the reference standard ADC (ADC_{IVIM}) for all of our experiments.

II.B.2. Regions of interest annotation

Abdominal organs, including the liver, spleen, and kidneys, were entirely segmented using the semiautomatic ITK-SNAP software tool[29] to define the ROI for ADC calculations. The initial manual annotation and the semiautomatic segmentation were performed on the DW-MRI image with *b*-value = 5 s/mm^2.The kidneys were further separated into the cortex and medulla regions using graph min-cut segmentation[30] based on ADC_{IVIM} values derived from their respective diffusivity properties.[31]

II.B.3. Simulated data experiment

DW-MRI data were simulated from the estimated parametric maps at each voxel using Eq. (1) with *b*-values in the following ranges: 0–300 s/mm^2 with gaps of 25 s/mm^2, 400, and 600–1200 s/mm^2 with gaps of 25 s/mm^2.

Images were corrupted by Rician noise with each channel Gaussian noise of $\mu = 0$ and $\sigma = 8$ representing the actual noise level observed in clinical DW-MRI.

Next, the commonly used monoexponential diffusion model[1]

$$s_i = s_0\exp(-b_i \mathrm{ADC}) \quad (2)$$

was fitted to the simulated images using the following three estimators:

1. Two *b*-values estimator (ADC_2):[1,32]

$$\frac{\ln s_1 - \ln s_2}{b_2 - b_1} = \mathrm{ADC} \quad (3)$$

TABLE I. Summary statistics of IVIM and ADC values for each organ and ADC estimation method.

	F	D^*[a]	$D(\mathrm{ADC_{IVIM}})$[a]	$\mathrm{ADC_2}$[a,b]	$\mathrm{ADC_3}$[a,b]	$\mathrm{ADC_R}$[a,b]
Liver	0.26 ± 0.04	27.4 ± 3.5	1.1 ± 0.1	1.1 ± 0.1	1.1 ± 0.1	1.1 ± 0.1
Kidney cortex	0.14 ± 0.03	22.2 ± 3.8	1.9 ± 0.1	1.9 ± 0.05	1.9 ± 0.1	1.9 ± 0.1
Kidney medulla	0.35 ± 0.07	22.2 ± 7.7	1.3 ± 0.1	1.5 ± 0.1	1.4 ± 0.1	1.5 ± 0.2
Spleen	0.14 ± 0.05	19.6 ± 4.2	0.9 ± 0.1	0.9 ± 0.1	0.9 ± 0.1	0.9 ± 0.1

Note: Data are means ± standard deviations.
[a]Data is in units of $\mu m^2/ms$.
[b]ADC calculated with $b_{min} = 270$ s/mm^2 and $b_{max} = 800$ s/mm^2. For $\mathrm{ADC_3}$ and $\mathrm{ADC_R}$ additional middle b-value = 400 s/mm^2 was used.

where b_1, b_2 are the b-values used to acquire the signal s_1, s_2, and ADC is the unknown model parameter.

2. Least-squares estimator ($\mathrm{ADC_3}$) with three b-value images:[25]

$$[s_0, \mathrm{ADC}] = \arg\min_{s_0,\mathrm{ADC}} \sum_{i=1}^{N} (s_i - s_0 \exp(-b_i \mathrm{ADC}))^2, \quad (4)$$

where b_i is the b-value used to acquire the signal s_i; N is the number of b-value images (three in our case); and s_0, ADC are the unknown model parameters. The singular value decomposition method was used to solve the derived linear system.

3. Maximum likelihood estimator with Rician noise model ($\mathrm{ADC_R}$) with three b-value images.[25]

$$[s_0, \mathrm{ADC}] = \arg\max_{\mathrm{ADC},s_0} \sum_{i=1}^{N} \ln I_0 \left(\frac{s_i (s_0 \exp(-b_i \mathrm{ADC}))}{\sigma_{R_i}^2} \right) - \sum_{i=1}^{N} \left(\frac{(s_0 \exp(-b_i \mathrm{ADC}))^2}{2\sigma_{R_i}^2} \right), \quad (5)$$

where I_0 is the modified Bessel function of the first kind with order zero.

Initial estimates of the model parameters were obtained with the least squares estimator Eq. (4). Noise variance was estimated using a predefined background region and Eq. (5) was maximized using the BOBYQA nonlinear optimization algorithm.[33] Both the values of the IVIM parameters and the ADC estimates were averaged over each organ. We aimed to find the b-values b_{min} and b_{max} that minimize the average relative root mean squared error (RRMS) between the $\mathrm{ADC_{IVIM}}$ and the ADC calculated with b_{min} and b_{max} over the J subjects

$$[b_{min}, b_{max}] = \arg\min_{b_{min},b_{max}} \frac{1}{J} \sum_{j=1}^{J} \sqrt{100 \times \left(\frac{\mathrm{ADC_{IVIM}} - \mathrm{ADC}(b_{min}, b_{max})}{\mathrm{ADC_{IVIM}}} \right)^2} \quad (6)$$

We found the b_{min}, b_{max} that minimize Eq. (6) by performing an exhaustive search over a lower b-value range of b_{min} = [0–300 s/mm^2], and a b_{max} = [600–1200 s/mm^2] with gaps of 25 s/mm^2. In turn, we determined the optimal combination of b-values that provide perfusion-insensitive ADC estimates from a *minimum* duration acquisition for each estimator ($\mathrm{ADC_2}$, $\mathrm{ADC_3}$, $\mathrm{ADC_R}$) and organ. For the estimators that require three b-value images [Eqs. (4) and (5)], we used the additional b-value = 400s/mm^2 as the middle b-value. This simulation study also enabled us to evaluate the effect of b-value choice on ADC estimation for very high b-value images (>800 s/mm^2) that were not part of the original clinical acquisition.

II.B.4. In vivo data experiment

Next, we fitted the monoexponential diffusion model [Eq. (2)] to the acquired DW-MRI data using the three estimators described above [Eqs. (3)–(5)]. Sets of b-value images (in pairs and triplets) covering the lower b-value range of 5–270 s/mm^2 and the higher b-value range of 600–800 s/mm^2 from the acquired DW-MRI data were used.

We found the b-values b_{min} and b_{max} that minimize the average relative root mean squared error over the J subjects between the $\mathrm{ADC_{IVIM}}$ and the ADC calculated with b_{min} and b_{max} [Eq. (6)] by performing an exhaustive search over pairs of b_{min} and b_{max} from the acquired DW-MRI data for each estimator ($\mathrm{ADC_2}$, $\mathrm{ADC_3}$, $\mathrm{ADC_R}$) and organ, respectively.

III. RESULTS

Table I depicts the summary statistics for the IVIM parameters and the ADC values calculated with $b_{min} = 270$ s/mm^2 and $b_{max} = 800$ s/mm^2 for each organ. The greatest difference between the $\mathrm{ADC_{IVIM}}$ and the estimated ADC using the monoexponential model was observed in the medulla of the kidney, which has the highest perfusion-fraction (f) value as compared to the other organs.

Figure 1 presents ADC maps calculated with the $\mathrm{ADC_2}$ estimator using b_{min} of 0,100,200 s/mm^2 and $b_{max} = 800$ s/mm^2 along with their signal decay curves. As the b_{min} increases, the discrepancy between the ADC model and the slow-diffusion component of the signal decay decreases.

III.A. Simulation experiments

Figure 2 presents the RRMS surfaces as a function of b_{min} and b_{max} for each organ and estimator as calculated from the simulated DW-MRI data. The RRMS between $\mathrm{ADC_{IVIM}}$ and $\mathrm{ADC_2}$, $\mathrm{ADC_3}$, and $\mathrm{ADC_R}$ decreases as b_{min} increases. The effect of increasing the b_{max} also improves the RRMS. However, b_{min} has relatively greater influence. As hypothesized, the RRMS between $\mathrm{ADC_{IVIM}}$ and $\mathrm{ADC_2}$, $\mathrm{ADC_3}$, and $\mathrm{ADC_R}$ is greater in high perfusivity organs (i.e., the liver and the

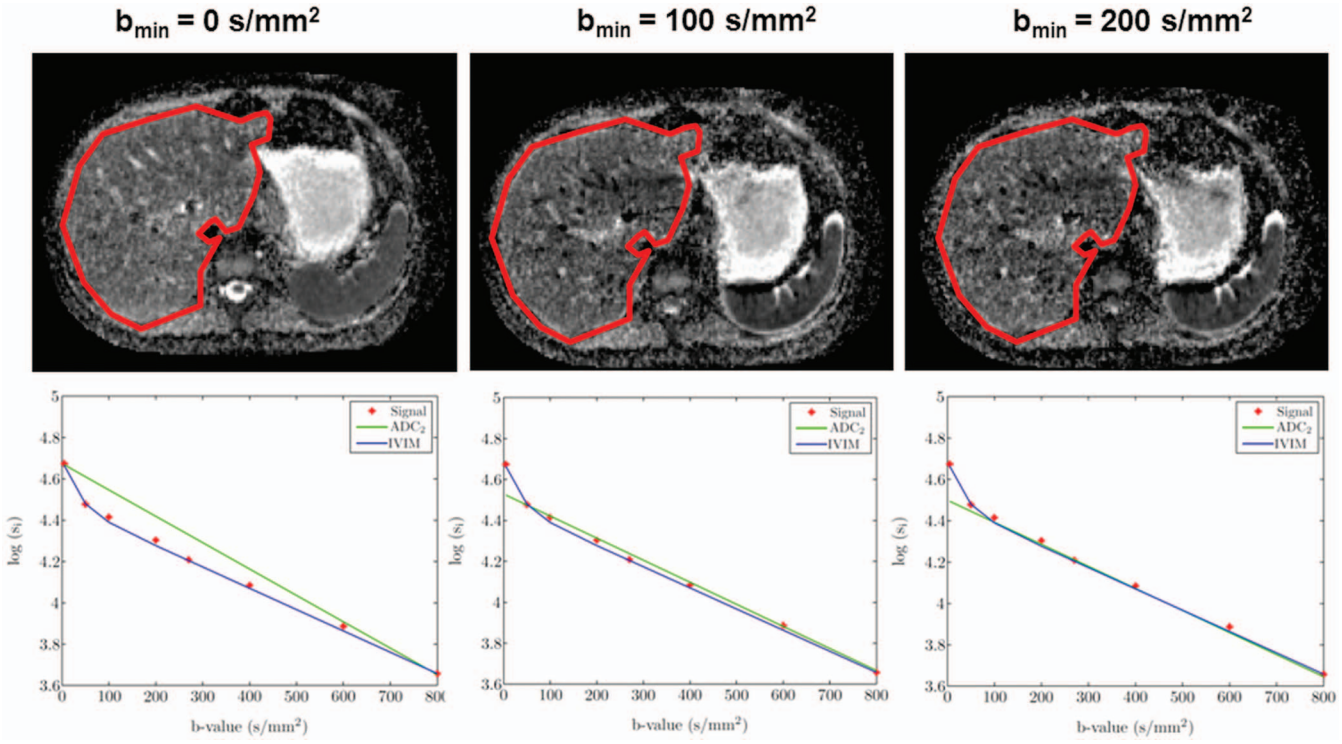

FIG. 1. Representative ADC maps (first row) and liver (encircled) signal-decay plots (second row) organized according to the minimal *b*-value used to calculate the ADC. The ADC maps were calculated using the ADC_2 estimator with fixed $b_{max} = 800$ s/mm^2 and varying b_{min}. The discrepancy between the ADC_2 and the slow-diffusion component of the IVIM model (ADC_{IVIM}) decreases as the b_{min} increases.

medulla of the kidney) than in low perfusivity organs (i.e., the cortex of the kidney and the spleen).

Table II summarizes sets of *b*-values (in pairs and triplets) that minimize the RRMS between the reference standard ADC_{IVIM} and the ADC values. These *b*-value sets were calculated using the three estimators being evaluated for each organ along with their RRMS value. The minimal RRMS obtained using the ADC_3 estimator with $b_{min} = 300$ s/mm^2 and $b_{max} = 1200$ s/mm^2. The ADC_R estimator has the greatest discrepancy between the reference standard ADC_{IVIM} and the estimated ADC values.

To assess the contribution of the perfusion compartment in the DW-MRI signal decay to the inaccurate estimation of the ADC; we evaluated the correlation between the *f* values for each organ and patient, and the minimal RRMS obtained by each ADC estimator. Table III shows that for all estimators, the RRMS strongly correlates with the *f* values.

III.B. *In vivo* experiments

Figure 3 presents the RRMS surfaces as a function of b_{min} and b_{max} for each organ and estimator as calculated from the *in vivo* DW-MRI data. The RRMS between ADC_{IVIM} and ADC_2, ADC_3, and ADC_R decreases as b_{min} increases. The effect of increasing the b_{max} also improves the RRMS. However, b_{min} has relatively greater influence. As also seen in the simulation results, the RRMS between ADC_{IVIM} and ADC_2, ADC_3, and ADC_R is greater in high perfusivity organs (i.e., the liver and the medulla of the kidney) than in low perfusivity organs (i.e., the cortex of the kidney and the spleen).

Table IV shows the sets of *b*-values (pairs and triplets) that minimize the RRMS between the reference standard ADC_{IVIM} and the ADC values calculated with the three estimators being evaluated for each organ along with their RRMS value. The minimal RRMS obtained using the ADC_3 estimator with $b_{min} = 270$ s/mm^2 and $b_{max} = 800$ s/mm^2.

For all organs, the ADC_3 calculated with $b_{min} = 270$ s/mm^2 and $b_{max} = 800$ s/mm^2 provides a relatively accurate (i.e., RRMS error $< 7\%$) estimation of the ADC.

IV. DISCUSSION

Our study demonstrates the effect of the perfusion component in the DW-MRI signal decay on ADC measurements from short-duration DW-MRI acquisitions. While previous studies show the effect of the minimal *b*-value used for monoexponential ADC calculations due to the inclusion of perfusion-related signal decay;[19,31] the rigorous optimization of the *b*-values used in short-duration DW-MRI with available ADC estimators has not been previously explored.

Our simulation results suggest that perfusion-insensitive ADC measurements can be obtained by using short-duration DW-MRI with $b_{min} = 300$ s/mm^2 and $b_{max} = 1200$ s/mm^2. However, increasing the b_{max} to 1200 s/mm^2 may both reduce the signal-to-noise ratio in the DW-MRI image *and* create greater distortion because of the larger TE required. Our *in vivo* experiments show that by combining $b_{min} = 270$ s/mm^2 and $b_{max} = 800$ s/mm^2 we can obtain adequate perfusion-insensitive ADC measurements with short-duration DW-MRI *without* increasing the b_{max} beyond optimal levels. Our

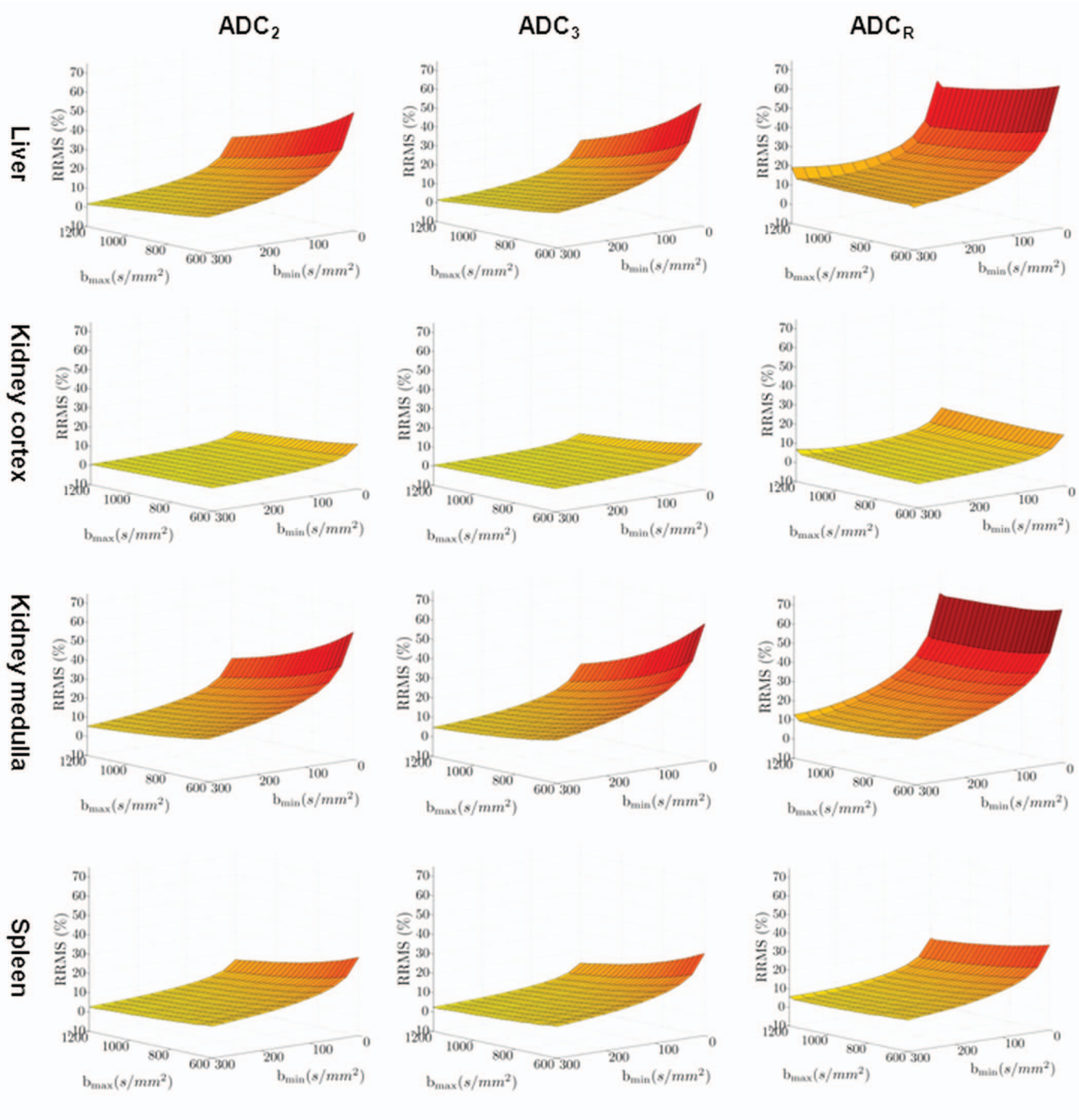

FIG. 2. The relative root mean squared error surface between the ADC estimates from the simulated DW-MRI data and the reference standard ADC_{IVIM} as a function of the b_{min} and b_{max}. The surfaces are organized according to the organ (rows) and the ADC estimator (columns).

TABLE II. Recommended pairs and triplets of *b*-values for each organ and ADC estimation method.

	ADC_2		ADC_3		ADC_R	
	b-values	RRMS %	*b*-values	RRMS %	*b*-values	RRMS %
Liver	300,1200	1.8	300,400,1200	1.5	300,400,1175	12.2
Kidney cortex	300,1200	0.6	300,400,1200	0.6	300,400,600	2.66
Kidney medulla	300,1200	5.4	300,400,1200	4.8	300,400,1075	10
Spleen	300,1175	2.6	300,400,1175	2.3	300,400,1175	4.7

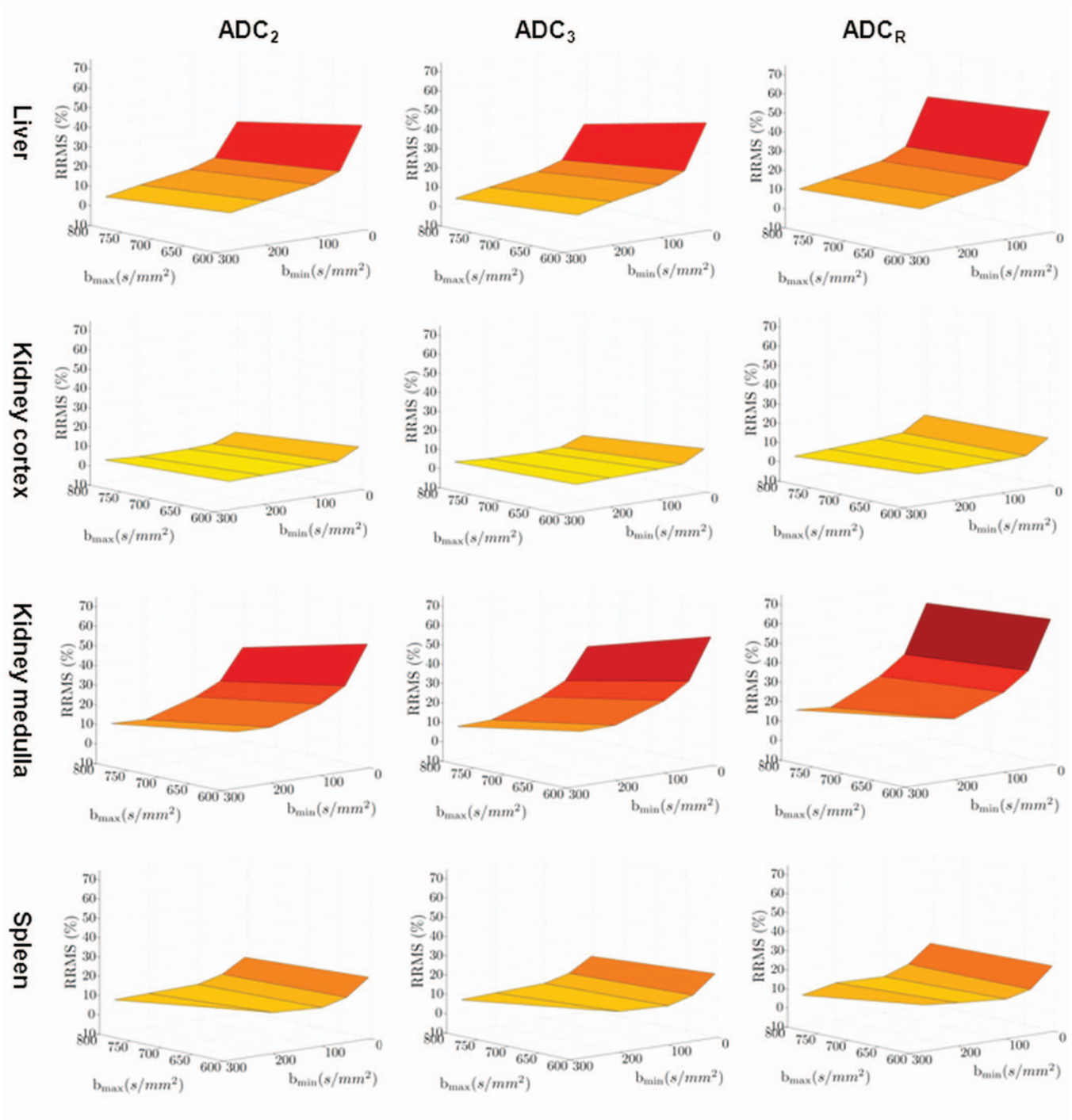

FIG. 3. The relative root mean squared error surface between the ADC estimates from the *in vivo* DW-MRI data and the reference standard ADC_{IVIM} as a function of the b_{min} and b_{max}. The surfaces are organized according to the organ (rows) and the ADC estimator (columns).

TABLE III. Correlation analysis between the fast-diffusion fraction (f) and the optimal RRMS obtained by the ADC estimators.

	r	P
ADC_2	0.79	0.002
ADC_3	0.78	0.003
ADC_R	0.83	>0.001

findings also suggest that increases in b_{min} have a greater impact on the accuracy of ADC estimation than increases in b_{max} do. Moreover, our study shows a strong correlation between the error in perfusion-insensitive ADC estimation and the actual contribution of the fast-diffusion compartment to the DW-MRI signal decay. By comparing the errors in ADC estimations to the existing estimation methods, we were able to show that ADC_R (Ref. 25) is more sensitive to perfusion

TABLE IV. Recommended pairs and triplets of *b*-values for each organ and ADC estimation method based on the *in vivo* data.

	ADC_2		ADC_3		ADC_R	
	b-values	RRMS %	*b*-values	RRMS %	*b*-values	RRMS %
Liver	270,800	3.5	270,400,800	3.1	270,400,800	9.1
Kidney cortex	200,800	1	100,400,800	1	270,400,800	1.8
Kidney medulla	200,800	8.6	270,400,800	6.8	200,400,800	13.4
Spleen	270,800	6.7	270,400,800	6.1	270,400,800	5.6

effects than are ADC_2 (Refs. 1 and 32) and ADC_3 (Ref. 25), respectively.

Our findings are of particular interest for detecting abdominal pathology in applications where a specific patient's ADC is compared to normative ADC values. Further, our data will aid in calibrating ADC estimates for assessing response-to-therapy, especially where ADC calculations have been performed in clinical practice using different ranges of *b*-values.

Our study had two significant limitations: First, to keep the imaging variables as constant and homogenous as possible, we performed all imaging experiments on the same 1.5 T system from a single vendor. This ideal scenario may not reflect the actual effect of the choice of *b*-values on DW-MRI data acquired with various field strengths or with systems from different vendors. Second, although our simulation experiments used very large and densely sampled ranges of *b*-values, we were forced, in part because of the *in vivo* nature of our second experiment, and in part because of scanning time limitations, to use a fixed, small set of *b*-values rather than exhaustively perform ADC calculations with all possible choices of *b*-values.

In conclusion, we have numerically identified the appropriate range of *b*-values that should be used in monoexponential ADC estimations relative to existing ADC estimation methods. By comparing monoexponential ADC estimates to perfusion-insensitive reference-standard ADC_{IVIM} for multiple organs, we have shown the feasibility of obtaining relatively accurate perfusion-insensitive ADC measurements using the monoexponential model with a fixed range of *b*-values for multiple organs using short-duration DW-MRI acquisition. In addition, we have identified the extent of errors in estimating ADC for each organ and likewise, have identified the best method for estimating a given choice of *b*-values.

ACKNOWLEDGMENT

This investigation was supported in part by NIH grants (Grant Nos. R01 RR021885, R01 EB008015, R03 EB008680, and R01 LM010033). The authors thank Nancy Drinan for her valuable support in editing this manuscript.

[a]Author to whom correspondence should be addressed. Electronic mail: moti.freiman@childrens.harvard.edu; Telephone: +1-617-255-3755; Fax: +1 617-730-4644.

[1]E. O. Stejskal and J. E. Tanner, "Spin diffusion measurements: spin-echo in the presence of a time dependent field gradient," J. Chem. Phys. **42**, 288–292 (1965).

[2]S. Gumustas, N. Inan, H. T. Sarisoy, Y. Anik, A. Arslan, E. Ciftci, G. Akansel, and A. Demirci, "Malignant versus benign mediastinal lesions: quantitative assessment with diffusion weighted MR imaging," Eur Radiol. **21**, 2255–2260 (2011).

[3]H. A. Vargas, O. Akin, T. Franiel, Y. Mazaheri, J. Zheng, C. Moskowitz, K. Udo, J. Eastham, and H. Hricak, "Diffusion-weighted endorectal MR imaging at 3 T for prostate cancer: Tumor detection and assessment of aggressiveness," Radiology **259**, 775–784 (2011).

[4]O. Dudeck, M. Zeile, D. Pink, M. Pech, P.-U. Tunn, P. Reichardt, W.-D. Ludwig, and B. Hamm, "Diffusion-weighted magnetic resonance imaging allows monitoring of anticancer treatment effects in patients with soft-tissue sarcomas," J. Magn. Reson. Imaging **27**, 1109–1113 (2008).

[5]C. L. Eccles, E. A. Haider, M. A. Haider, S. Fung, G. Lockwood, and L. A. Dawson, "Change in diffusion weighted MRI during liver cancer radiotherapy: Preliminary observations," Acta Oncol. **48**, 1034–1043 (2009).

[6]D. M. Koh, M. Blackledge, D. J. Collins, A. R. Padhani, T. Wallace, B. Wilton, N. J. Taylor, J. J. Stirling, R. Sinha, P. Walicke, M. O. Leach, I. Judson, and P. Nathan, "Reproducibility and changes in the apparent diffusion coefficients of solid tumours treated with combretastatin A4 phosphate and bevacizumab in a two-centre phase I clinical trial," Eur. Radiol. **19**, 2728–2738 (2009).

[7]B. Taouli and D.-M. Koh, "Diffusion-weighted MR imaging of the liver," Radiology **254**, 47–66 (2010).

[8]S. Bonekamp, M. S. Torbenson, and I. R. Kamel, "Diffusion-weighted magnetic resonance imaging for the staging of liver fibrosis," J. Clin. Gastroenterol. **45**, 885–892 (2011).

[9]K. Fujimoto, T. Tonan, S. Azuma, M. Kage, O. Nakashima, T. Johkoh, N. Hayabuchi, K. Okuda, T. Kawaguchi, M. Sata, and A. Qayyum, "Evaluation of the mean and entropy of apparent diffusion coefficient values in chronic hepatitis C: correlation with pathologic fibrosis stage and inflammatory activity grade," Radiology **258**, 739–748 (2011).

[10]S. Kiryu, K. Dodanuki, H. Takao, M. Watanabe, Y. Inoue, M. Takazoe, R. Sahara, K. Unuma, and K. Ohtomo, "Free-breathing diffusion-weighted imaging for the assessment of inflammatory activity in Crohn's disease," J. Magn. Reson. Imaging **29**, 880–886 (2009).

[11]A. Oto, A. Kayhan, J. T. Williams, X. Fan, L. Yun, S. Arkani, and D. T. Rubin, "Active Crohn's Disease in the small bowel: Evaluation by diffusion weighted imaging and quantitative dynamic contrast enhanced MR imaging," J. Magn. Reson. Imaging **33**, 615–624 (2011).

[12]J. F. Kallehauge, K. Tanderup, S. Haack, T. Nielsen, L. P. Muren, L. Fokdal, J. C. Lindegaard, and E. M. Pedersen, "Apparent Diffusion Coefficient (ADC) as a quantitative parameter in diffusion weighted MR imaging in gynecologic cancer: Dependence on *b*-values used," Acta Oncol. **49**, 1017–1022 (2010).

[13]N. H. Peters, K. L. Vincken, M. A. van den Bosch, P. R. Luijten, W. P. Mali, and L. W. Bartels, "Quantitative diffusion weighted imaging for differentiation of benign and malignant breast lesions: the influence of the choice of *b*-values," J. Magn. Reson. Imaging **31**, 1100–1105 (2010).

[14]R. Girometti, A. Furlan, G. Esposito, M. Bazzocchi, G. Como, F. Soldano, M. Isola, P. Toniutto, and C. Zuiani, "Relevance of *b*-values in evaluating liver fibrosis: a study in healthy and cirrhotic subjects using two single-shot spin-echo echo-planar diffusion-weighted sequences," J. Magn. Reson. Imaging **28**, 411–419 (2008).

[15]A. Lemke, F. B. Laun, D. Simon, B. Stieltjes, and L. R. Schad, "An *in vivo* verification of the intravoxel incoherent motion effect in diffusion-

weighted imaging of the abdomen," Magn. Reson. Med. **64**, 1580–1585 (2010).
[16]D. M. Koh, D. J. Collins, and M. R. Orton, "Intravoxel incoherent motion in body diffusion-weighted MRI: reality and challenges," AJR, Am. J. Roentgenol. **196**, 1351–1361 (2011).
[17]D. Le Bihan, E. Breton, D. Lallemand, M. L. Aubin, J. Vignaud, and M. Laval-Jeantet, "Separation of diffusion and perfusion in intravoxel incoherent motion MR imaging," Radiology **168**, 497–505 (1988).
[18]A. Lemke, B. Stieltjes, L. R. Schad, and F. B. Laun, "Toward an optimal distribution of *b*-values for intravoxel incoherent motion imaging," Magn. Reson. Imaging **29**, 766–776 (2011).
[19]I. Yamada, W. Aung, Y. Himeno, T. Nakagawa, and H. Shibuya, "Diffusion coefficients in abdominal organs and hepatic lesions: evaluation with intravoxel incoherent motion echo-planar MR imaging," Radiology **210**, 617–623 (1999).
[20]A. R. Padhani, G. Liu, D. M. Koh, T. L. Chenevert, H. C. Thoeny, T. Takahara, A. Dzik-Jurasz, B. D. Ross, M. Van Cauteren, D. Collins, D. A. Hammoud, G. J. S. Rustin, B. Taouli, and P. L. Choyke, "Diffusion-weighted magnetic resonance imaging as a cancer biomarker: consensus and recommendations," Neoplasia **11**, 102–125 (2009).
[21]N. Papanikolaou, S. Gourtsoyianni, S. Yarmenitis, T. Maris, and N. Gourtsoyiannis, "Comparison between two-point and four-point methods for quantification of apparent diffusion coefficient of normal liver parenchyma and focal lesions. Value of normalization with spleen," Eur. J. Radiol. **73**, 305–309 (2010).
[22]R. A. Clarke, P. Scifo, G. Rizzo, F. Dell'Acqua, G. Scotti, and F. Fazio, "Noise correction on Rician distributed data for fibre orientation estimators," IEEE Trans. Med. Imaging **27**, 1242–1251 (2008).
[23]P. A. Taylor and B. Biswal, "Geometric analysis of the b-dependent effects of Rician signal noise on diffusion tensor imaging estimates and determining an optimal *b*-value," Magn. Reson. Imaging **29**, 777–788 (2011).
[24]J. L. Andersson, "Maximum a posteriori estimation of diffusion tensor parameters using a Rician noise model: why, how and but," Neuroimage **42**, 1340–1356 (2008).
[25]S. Walker-Samuel, M. Orton, L. D. McPhail and S. P. Robinson, "Robust estimation of the apparent diffusion coefficient (ADC) in heterogeneous solid tumors," Magn. Reson. Med. **62**, 420–429 (2009).
[26]T. E. Conturo, R. C. McKinstry, E. Akbudak, and B. H. Robinson, "Encoding of anisotropic diffusion with tetrahedral gradients: a general mathematical diffusion formalism and experimental results," Magn. Reson. Med. **35**, 399–412 (1996).
[27]R. V. Mulkern, S. Vajapeyam, R. L. Robertson, P. A. Caruso, M. J. Rivkin, and S. E. Maier, "Biexponential apparent diffusion coefficient parametrization in adult vs newborn brain," Magn. Reson. Imaging **19**, 659–668 (2001).
[28]M. Freiman, S. D. Voss, R. V. Mulkern, J. M. Perez-Rossello, and S. K. Warfield, "Quantitative body DW-MRI biomarkers uncertainty estimation using unscented wild-bootstrap," Med. Image Comput. Comput. Assist. Interv. **14**, 73–80 (2011).
[29]P. A. Yushkevich, J. Piven, H. C. Hazlett, R. G. Smith, S. Ho, J. C. Gee, and G. Gerig, "User-guided 3D active contour segmentation of anatomical structures: significantly improved efficiency and reliability," Neuroimage **31**, 1116–1128 (2006).
[30]Y. Boykov and G. Funka-Lea, "Graph cuts and efficient N-D image segmentation," Int. J. Comput. Vis. **70**, 109–131 (2006).
[31]J. L. Zhang, E. E. Sigmund, H. Chandarana, H. Rusinek, Q. Chen, P. H. Vivier, B. Taouli, and V. S. Lee, "Variability of renal apparent diffusion coefficients: limitations of the monoexponential model for diffusion quantification," Radiology **254**, 783–792 (2010).
[32]D. M. Koh and D. J. Collins, "Diffusion-weighted MRI in the body: Applications and challenges in oncology," AJR, Am. J. Roentgenol. **188**, 1622–1635 (2007).
[33]M. J. D. Powell, "Developments of NEWUOA for minimization without derivatives," IMA J. Numer. Anal. **28**, 649–664 (2008).